Article

Two-Dimensional Superdegeneracy and Structure–Magnetism Correlations in Strong Ferromagnet, MnGa

Sang-Hwan Kim, Magnus Bostrm, and Dong-Kyun Seo

J. Am. Chem. Soc., **2008**, 130 (4), 1384-1391 • DOI: 10.1021/ja0765924

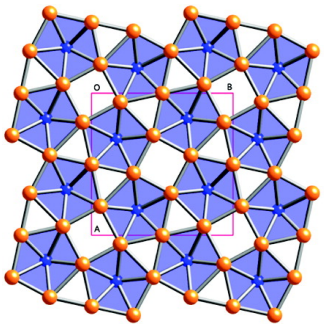

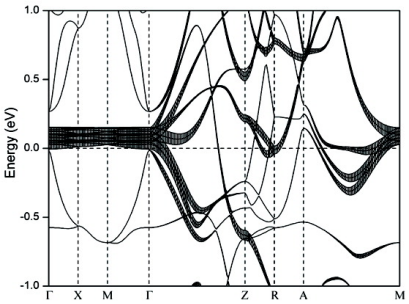

More About This Article

Additional resources and features associated with this article are available within the HTML version:

- Supporting Information
- Links to the 1 articles that cite this article, as of the time of this article download
- Access to high resolution figures
- Links to articles and content related to this article
- Copyright permission to reproduce figures and/or text from this article

View the Full Text HTML

J|A|C|S
ARTICLES
Published on Web 01/08/2008

Two-Dimensional Superdegeneracy and Structure−Magnetism Correlations in Strong Ferromagnet, Mn_2Ga_5

Sang-Hwan Kim, Magnus Boström,[†] and Dong-Kyun Seo*

Department of Chemistry and Biochemistry, Arizona State University, Tempe, Arizona 85287-1604, and European Synchrotron Radiation Facility (ESRF), BP 220, 38043 Grenoble Cedex 9, France

Received August 31, 2007; E-mail: dseo@asu.edu

Abstract: The ferromagnetic intermetallic compound Mn_2Ga_5 has been synthesized and characterized by single-crystal X-ray diffraction study and by magnetic property measurements. The compound, with the Mn_2Hg_5-type structure, exhibits a saturated magnetic moment of 2.71 μ_B per formula unit with $T_C \approx 450$ K. The electronic structure of the compound was analyzed by employing FPLO, LMTO, and the extended Hückel tight-binding calculations. The nonmagnetic electronic structure of Mn_2Ga_5 reveals remarkably flat degenerate (superdegenerate) bands in the vicinity of the Fermi level but only in the a^*b^*-plane of the Brillouin zone. The resulting high density of the states at the Fermi level, DOS(E_F), is consistent with the Stoner condition for the observed itinerant electron ferromagnetism. Detailed orbital analysis shows an intriguing structure−magnetism correlation, as the superdegeneracy is found to be a consequence of the unique atomic arrangement and bond angles in the structure.

Introduction

Magnetic intermetallics have attracted a significant interest recently because of their interesting physical phenomena[1−5] associated with itinerant electron magnetism. Itinerant electron magnets (or simply "metallic magnets") show a metallic conductivity and exhibit (usually) localized magnetic moments whose magnetic interactions are mediated by conducting electrons. Since the delocalized conducting electrons are also responsible for the metallic conductivity, they play an essential role in spin-dependent electrical conduction.[6−10] That is, the electrical transport process can be affected by the magnetic states of the compounds which can be manipulated in turn by external input such as the changes in applied magnetic field strength, temperature, or pressure. What is relevant to chemists is that those delocalized electrons are also responsible to the chemical bonding and structural stabilization of the intermetallics, and thus the magnetic intermetallics are an ideal playground in exploring the effect of chemical bonding on itinerant electron magnetism.

What distinguishes magnetic intermetallics from other magnetic compounds such as magnetic insulators or organic/organometallic molecular magnets is that their complicated bonding patterns generally hinder us from *a priori* prediction of their magnetic properties to the same level of details without employing first-principle electronic band structure calculations. Nonetheless, one common starting point is that magnetic properties of intermetallics are also determined by the electronic bands near the Fermi level (called "frontier bands") whose feature is in turn governed by the chemical structure and bonding of the compounds. In the continuous energy structure of intermetallics, each energy level is doubly occupied up to the Fermi level, when the electron repulsion between the paired electrons is small compared to the energy stabilization gained by the double occupation. Under a certain circumstance described later, however, the electron repulsion becomes strong enough so that some of the frontier bands are singly occupied as spin polarization takes place in the electronic structure.[6,7] The consequent inequivalency in orbital shapes and energies in different spin channels provides a nonzero magnetic moment in the magnetic state of the compound. In a simplistic and yet quantitative model, such spontaneous spin polarization is predicted from the *nonmagnetic* band structure of a metal when the metal satisfies the Stoner condition;[6,7] $I \times \mathrm{DOS}(E_F) > 1$, where I and DOS(E_F) are the Stoner (exchange) parameter and the density of states (DOS) at the Fermi level (E_F) in the nonmagnetic state, respectively.[11−13] The Stoner parameters are characteristic of atoms, and only DOS(E_F) reflects the electronic

[†] European Synchrotron Radiation Facility (ESRF).

(1) De Groot, R. A.; Mueller, F. M.; Van Engen, P. G.; Buschow, K. H. J. *Phys. Rev. Lett.* **1983**, *50*, 2024.
(2) Kim, S.-H.; Seo, D.-K.; Kremer, R. K.; Kohler, J.; Villesuzanne, A.; Whangbo, M.-H. *Chem. Mater.* **2005**, *17*, 6338.
(3) Binasch, G.; Grünberg, P.; Saurenbach, F.; Zinn, W. *Phys. Rev. B: Condens. Mater. Phys.* **1989**, *39*, 4282.
(4) Baibich, M. N.; Broto, J. M.; Fert, A.; Nguyen Van Dau, F.; Petroff, F.; Eitenne, P.; Creuzet, G.; Friederich, A.; Chazelas, J. *Phys. Rev. Lett.* **1988**, *61*, 2472.
(5) Miller, G. J. *Chem. Soc. Rev.* **2006**, *35*, 799.
(6) Stoner, E. C. *Proc. R. Soc. London A* **1936**, *154*, 656.
(7) Stoner, E. C. *Proc. R. Soc. London A* **1938**, *165*, 372.
(8) Rhodes, P.; Wohlharth, E. P. *Proc. R. Soc. London A* **1963**, *273*, 247.
(9) Kübler, J. *Theory of Itinerant Electron Magnetism*; Oxford University Press: New York, 2000.
(10) Mohn, P. *Magnetism in the Solid State: An Introduction*; Springer: Berlin, 2006.
(11) Janak, J. F. *Phys. Rev. B: Condens. Mater. Phys.* **1977**, *16*, 255.
(12) Seo, D.-K. *J. Chem. Phys.* **2006**, *125*, 154105.
(13) Seo, D.-K.; Kim, S.-H. *Solid State Sci.* **2007**. In press.

10.1021/ja0765924 CCC: $40.75

Table 1. Single-Crystal Data of Mn_2Ga_5 and Structure Refinement Parameters

space group, Z	*P4/mbm* (no. 127), 2
formula weight	458.48
lattice parameters (Å)	$a = 8.8590(8)$, $c = 2.7094(5)$
ρ_{calcd} (g/cm^3)	3.580
μ (Mo Kα, cm^{-1})	65.1
R1, wR2[a]	0.0408, 0.0902

[a] $R1 = \sum||F_o| - |F_c||$, $wR2 = \{\sum[w(F_o^2 - F_c^2)]/\sum[w(F_o^2)^2]\}^{1/2}$.

nature of the metal and thus determines the possible occurrence of spin polarization in the metal.

Among the intermetallics containing transition metals such as Mn, Fe, or Co, p-metal-rich transition metal intermetallics have been of our interest because they are positioned at an extreme of the bonding spectrum. Because of their chemical composition with excess p-metal atoms, the structures of p-metal-rich transition metal intermetallics exhibit encapsulated transition metal atoms surrounded by a p-metal network. In such a coordination environment, the transition-metal d-orbitals must extensively participate in chemical bond formation and hence optimization of atomic arrangements in structure. Certainly, chemical bonding, delocalized or localized, favors electron pairing, which by definition prevents formation of a spontaneous magnetic moment. This is the familiar case of most p-metal-rich transition-metal intermetallics such as $MnGa_4$, $MnAl_6$, and $MnAl_{12}$, VAl_{10}, $CrGa_4$, $Mn_8Ga_{27.4}Zn_{13.6}$, $FeGa_4$, Co_2Al_5, Co_2Al_9, $NiAl_3$, and Cu_2FeAl_9 as well as many quasicrystals and their approximants.[14−21] The observed structure−magnetism correlation does fit well with the Stoner condition; as the bonding and antibonding bands become stabilized and destabilized, respectively, through bonding optimization, the DOS depletes at the Fermi level. Upon such relatively strong bonding optimization, the resulting small DOS(E_F) does not satisfy the Stoner condition, and hence, the compounds are nonmagnetic or weakly magnetic at best.

The title compound, Mn_2Ga_5, is quite intriguing in this regard, as it is known to show a strong ferromagnetism even at room temperature and exhibits a magnetic moment of 1.78 μ_B/Mn based on neutron diffraction studies.[22,23] In fact, the gallide is the only ferromagnetic compound that is thermodynamically stable in the Mn−Ga binary system. The known Mn-richer compounds are either ferrimagnetic or antiferromagnetic, except the metastable δ-MnGa.[14−16] Both of other known Ga-rich compounds, $MnGa_4$ and $MnGa_3$, are Pauli-paramagnetic, being consistent with the aforementioned behavior of the p-metal-rich transition metal intermetallics. While the Mn_2Ga_5 is located at the Mn-richer side in comparison to the other Ga-rich phase such as $MnGa_4$ and $MnGa_3$, the atomic ratio in its composition clearly indicates that Mn atoms are significantly outnumbered by Ga and hence are likely well surrounded by Ga atoms. Reportedly, the compound is isostructural to Mn_2Hg_5 in which Mn atoms are sandwiched by two Hg pentagonal rings as is the Fe atom in the ferrocene molecule with the eclipsed geometry. However, the single-crystal structure of the Mn_2Ga_5 has not been available yet for the details of the structure and for the studies of its magnetism. More critically, the reported magnetism of the Mn_2Ga_5 was in fact from a significantly Mn-deficient sample, $Mn_{1.85}Ga_5$ ($T_c = 521$ K), indicating a possible phase width,[23] but the existence of a stoichiometric compound itself has to be confirmed.

Table 2. Atomic Coordinates ($\times 10^4$ Å) and Isotropic Equivalent Displacement Parameters ($\times 10^3$ Å^2) for Mn_2Ga_5

	Wyck	x	y	z	U_{eq}[a]
Mn	4h	6782(3)	1782(3)	5000	6(1)
Ga(1)	2d	5000	0	0	7(1)
Ga(2)	8i	2046(2)	635(2)	0	8(1)

[a] U_{eq} is defined as a third of the trace of the orthogonalized $\mathbf{U}_{ij}$ tensor.

Table 3. Selected Bond Distances (Å) and Selected Bond Angles (deg) in Mn_2Ga_5

bond	distance (Å)	angle	(deg)
Ga(1)−Mn	2.611(3) × 4	Ga(1)−Mn−Ga(1)	62.51(8)
Ga(1)−Ga(2)	2.677(2) × 4	Ga(2)−Mn−Ga(2)	60.98(7)
Ga(1)−Ga(1)	2.709(1) × 2	Ga(2)−Mn−Ga(2)	60.98(7)
		Ga(2)−Mn−Ga(2)	59.31(5)
Ga(2)−Mn	2.670(3) × 2	Ga(2)−Mn−Ga(2)	59.31(5)
Ga(2)−Mn	2.738(2) × 2		
Ga(2)−Ga(2)	2.683(3) × 2		
Ga(2)−Ga(2)	2.709(1) × 2		
Ga(2)−Ga(2)	2.906(4) × 2		
Mn−Ga(1)	2.611(3) × 2		
Mn−Ga(2)	2.670(3) × 4		
Mn−Ga(2)	2.738(2) × 4		
Mn−Mn	2.709(1) × 2		

In our effort to elucidate the origin of the strong ferromagnetism of the compound, we report the synthesis of stoichiometric Mn_2Ga_5, structural determination via single-crystal X-ray crystallography, magnetic property measurements, and electronic structure analysis through first-principle electronic band structure calculations. On the basis of detailed electronic structure analysis, a remarkable superdegeneracy is discovered near the Fermi level in its electronic structure as the origin of the strong ferromagnetism of the compound. The subsequent orbital analysis shows a striking correlation between the chemical and electronic structures that is responsible to the magnetism of the Mn_2Ga_5. Furthermore, the discovery establishes an important connection of itinerant electron magnetism to other types of magnetism, namely, the significance of nonbonding transition metal orbitals.

Experimental Section

Synthesis. High purities of Ga (99.99%, Alfa Aesar) and Mn (dendritic pieces, 99.98%, Alfa Aesar) were used. The Mn pieces were cleaned by etching out the oxide layers on the surface in a HNO_3 solution (10 wt %). All the materials were handled in a nitrogen-filled glove box with a 0.1 ppm oxygen level. Both self-flux and solid-state methods were successful for the synthesis. In our self-flux route,[24] appropriate amounts of Mn (0.2 g) and Ga (1.8 g) metals were loaded into fused silica tubes, well-baked in vacuum, where crushed silica

(14) Matsui, T.; Suzuki, M.; Morii, K.; Nakayama, Y. *J. Appl. Phys.* **1993**, *73*, 6683.
(15) Yang, Z.; Li, J.; W, D.-S.; Zhang, K.; Xie, X. *J. Magn. Magn. Mater.* **1998**, *182*, 369.
(16) Gourdon, O.; Miller, G. J. *J. Solid State Chem.* **2003**, *173*, 137.
(17) De Laissardiére, G. T.; Nguyen Manh, D.; Magaud, L.; Julien, J. P.; Cyrot-Lackmann, F.; Mayou, D. *Phys. Rev. B: Condens. Mater. Phys.* **1995**, *52*, 7920.
(18) Häussermann, U.; Viklund, P.; Svensson, C.; Eriksson, S.; Berastegui, P.; Lidin, S. *Angew. Chem., Int. Ed.* **1999**, *38*, 488.
(19) Janot, C. *Quasicrystals: A Primer*, 2nd Ed.; Oxford University Press: Oxford, UK, 1994.
(20) Wu, L.-M.; Seo, D.-K. *J. Am. Chem. Soc.* **2004**, *126*, 4398.
(21) Blandin, A.; Friedel, J. *J. Phys. Rad.* **1959**, *20*, 160.
(22) Kitchingman, W. J.; Norman, P. L. *Acta Crystallogr.* **1972**, *B28*, 1311.
(23) Kitchingman, W. J.; Norman, P. L. *J. Appl. Cryst.* **1973**, *6*, 240.
(24) Boström, M.; Hovmöller, S. *J. Solid State. Chem.* **2000**, *153*, 398.

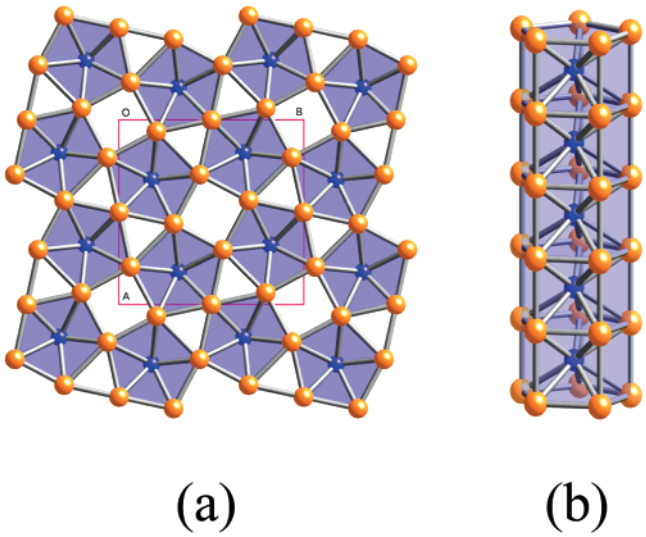

Figure 1. (a) [001] Projection view of the Mn_2Ga_5 crystal structure and (b) a $MnGa_5$ pentagonal column running along the *c*-axis. Blue: Mn. Orange: Ga. For convenience, the Mn−Mn bonds are omitted.

pieces were placed at the bottom as a filter supporter and a silica wool was situated as a filter on the top of the crushed pieces.[28,29] The fused silica tubes were then flame-sealed under vacuum ($\sim 10^{-6}$ Torr). The sealed tubes were placed in a vertical furnace, heated at 700 °C for 10 h, and then radiatively cooled down to 500 °C where they were kept for 3 days. Afterward, the tubes were taken out from the furnace, and the excess Ga liquid was filtered out immediately in a centrifuge at 4000 rpm for several minutes.

In the solid-state route, stoichiometric amounts of the elements were arc-melted in an argon-filled chamber with a zirconium oxygen-getter. Our experiences indicated that 5% excess Mn should be added for a stoichiometric product by compensating evaporation loss of Mn during the arc-melting. To ensure the homogeneity of the samples, the buttons were flipped over and then remelted several times. Then each button was placed in an evacuated and flame-sealed fused silica tube that was heated at 500 °C for 10 days and then quenched in ice water. In an alternative route, slowing the cooling process only resulted in decomposition of the target compound during cooling.

Powder X-ray diffraction studies of the bulk samples from both methods showed that the products were pure without impurities and the Bragg reflections were well matched with the simulated powder diffraction pattern from our single-crystal structure. Wave-dispersive electron microprobe analysis was carried out with a JEOL 8600 superprobe equipped with a four-wavelength dispersive spectrometer. The obtained composition, $Mn_{2.05(3)}Ga_{4.95(3)}$, also indicates that our samples were stoichiometric and the title compound does exist in a stoichiometric form.

Structural Determination and Magnetic Property Measurements. A silvery crystal of a square disk shape (ca. 0.03 × 0.03 × 0.01 mm^3) was mounted on a fine glass rod with an epoxy glue and was transferred to a Bruker-AXS Smart APEX CCD-equipped X-ray diffractometer. To check the crystal quality, a rotation photograph was first taken. Diffraction data were collected at 25 °C with monochromated Mo Kα radiation and were collected in a total of 1818 frames from three sets of 0.3° scans in ω at ϕ settings of 0, 120, and 240° with the exposure time of 30 s per frame. The SAINT subprogram in the SMART software package[25] was used to integrate the reflection intensities. Total 1234 reflections yielded in this process were merged into 95 independent reflections, out of which 90 had intensities greater than $2\sigma(I)$. The data were initially corrected for absorption by using the SADABS routine in the SAINT subprogram. The space group was determined by using the XPREP subprogram in the SHELXTL software package.[26] The initial model was obtained by the direct method. The full-matrix least-squares refinement converged at R(F) = 4.0%, wR2 = 8.3% and GOF = 1.49. The maximum and minimum residual peak and hole in the final ΔF map were 0.808 and −1.061 $e^-\cdot Å^{-3}$, respectively. The refined parameters are consistent with those of V_2Ga_5, which is also isostructural to Mn_2Hg_5 but closer to the title compound in the size of the nonmagnetic atoms (Ga vs Hg).[27] Some aspects of the data collection and refinement are listed in Table 1. The atomic positions and isotropic equivalent displacement parameters are provided in Table 2. Important interatomic distances and bond angles in the structure are given in Table 3. Magnetic properties were characterized on well-ground black powder samples with a Quantum Design MPMS SQUID magnetometer. The magnetization was measured at H = 10 kOe in the temperature range of 1.8 − 800 K. A hysteresis curve was obtained at 5 K by sweeping the magnetic field (1 1/2 cycles) from −10 to 10 kOe.

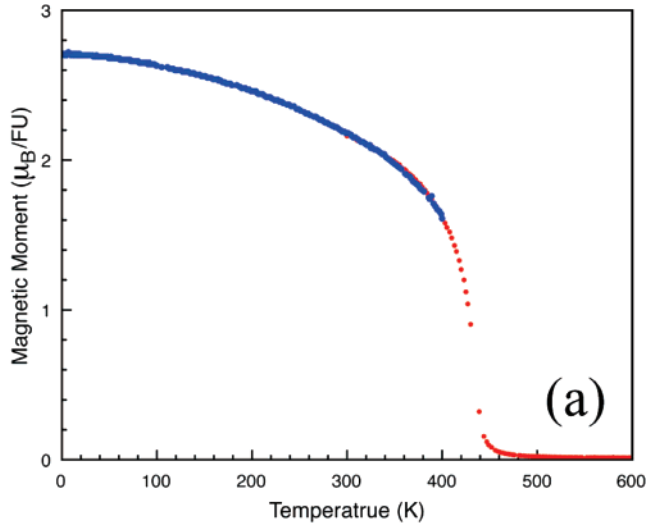

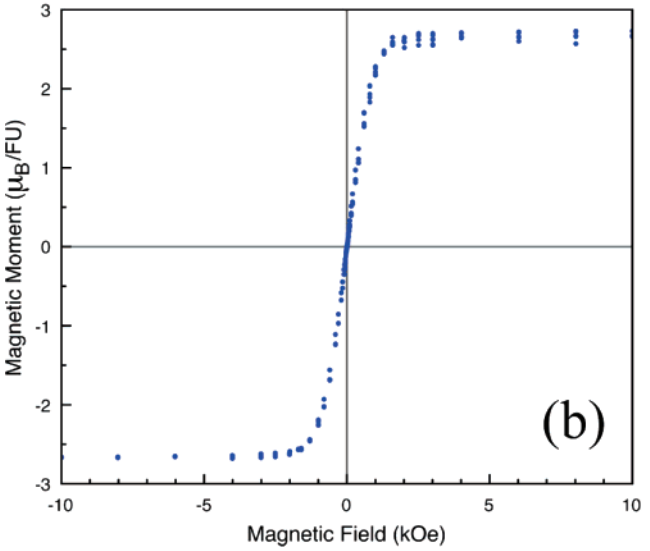

Figure 2. (a) Magnetization vs temperature at H = 10 kOe and (b) magnetization vs magnetic field at T = 5 K.

Electronic Structure Calculations. First-principle electronic band structures for the Mn_2Ga_5 were calculated with the tight-binding linear

(25) *SMART*; Bruker AXS, Inc.: Madison, WI, 1996.
(26) *SHELXTL*; Bruker AXS, Inc.: Madison, WI, 1997.
(27) Lobring, K. C.; Check, C. E.; Zhang, J.; Li, S.; Zheng, C.; Rogacki, K. *J. Alloys Compd*. **2002**, *347*, 72.
(28) Tank, R. W.; Jepsen, O.; Burckhardt. A.; Andersen, O. K. *TB-LMTO-ASA program*, Vers. 4.7c; Max-Planck-Institut für Festkörperforschung: Stuttgart, Germany, 1994.
(29) Barth, U.; Hedin, L. *J. Phys*. **1972**, *5*, 1629.

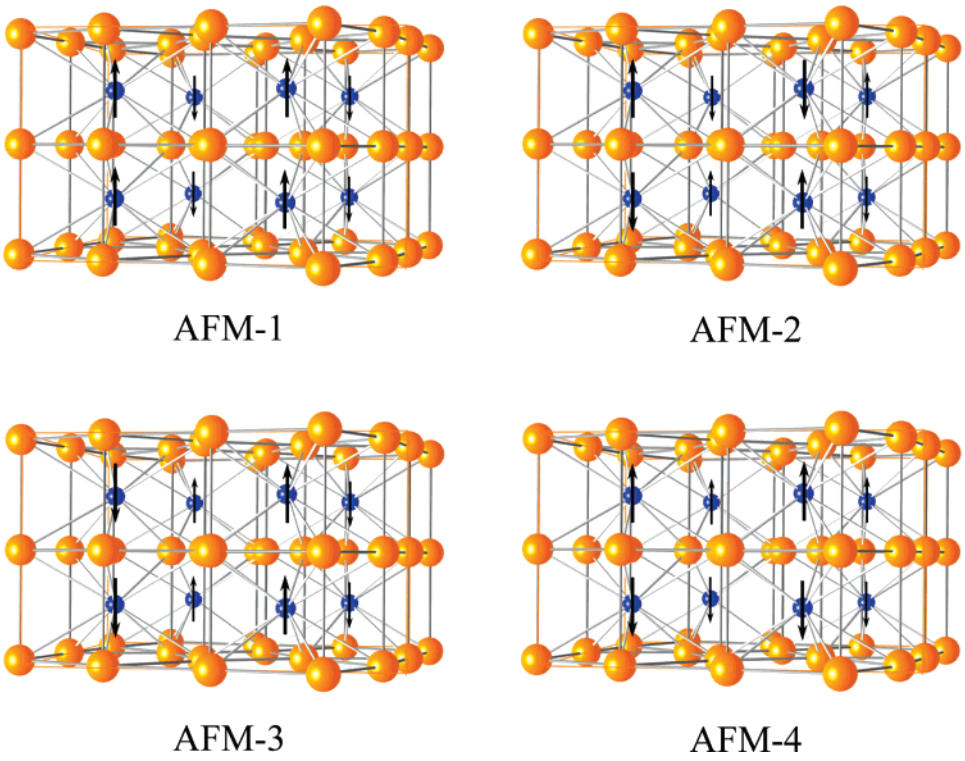

Figure 3. Four different AFM spin arrangements possible in the Mn_2Ga_5 structure. The unit cell is double along the *c*-axis to accommodate AFM spin arrangements in that direction. The up and down arrows indicate spin polarization densities of the opposite signs on the Mn atoms.

muffin-tin orbital (TB-LMTO) and full-potential local orbital (FPLO) methods by employing the local (spin) density approximation (L(S)-DA). The TB-LMTO calculations were carried out within atomic sphere approximation (ASA).[28] The von Barth-Hedin local exchange-correlation potential[29] was used for the L(S)DA, and the radial scalar relativistic Dirac equation was solved for obtaining the partial waves. No empty spheres were necessary to achieve space filling. A total of 100 irreducible *k*-points with a $6 \times 6 \times 18$ grid was used for Brillouin zone integrations by the tetrahedron method.[30,31] The basis set consisted of Mn-4s/4p/3d and Ga-4s/4p/[4d] orbitals. The orbital in brackets was treated with the downfolding technique.[32] Self-consistency was achieved within the total energy change smaller than 10^{-5} Rydberg.

The FPLO version 4 was used in our FPLO calculations. It employs a hydrogen-like atomic orbital basis set that is numerically optimized during the SCF procedure.[33] Perdew−Wang 92 parametrization[34] was used for the L(S)DA exchange-correlation functional in the scalar relativistic calculation. The tetrahedron method was applied for the integration of Brillouin zone in $6 \times 6 \times 8$ grid. The basis sets employed were Mn (4s, 4p, 3d) and Ga (4s, 4p, 3d) states. The lower-lying orbitals of the atoms were treated with a frozen core approximation. Fixed spin moment calculations and volume optimization were performed in the same way.

Orbital overlap integrals between Mn($3d_{xz}$) and Ga($4p_z$) in the extended Hückel approximation[35,36] were calculated using the CAESAR program package.[37] A weighted H_{ij} formula was used for the extended Hückel calculations, and the following atomic orbital energies and exponents were employed for the overlap integral calculations (H_{ii} = orbital energy, ζ = Slater exponent): Mn 3d, $H_{ii} = -8.7$ eV, $\zeta_1 = 5.15$ $\zeta_2 = 1.70$;[38] Ga 4p, $H_{ii} = -6.75$ eV, $\zeta = 1.55$.[39]

Results and Discussion

Structural Description and Magnetic Properties. Figure 1a shows a [001] projection view of the tetragonal structure of Mn_2Ga_5 (space group: *P4/mbm*; $a = 8.8590(8)$ Å, $c = 2.7094(5)$ Å, $Z = 2$). The structure exhibits a three-dimensional Ga network made up of two crystallographically different types of Ga atoms. Although the two Ga sites are inequivalent, their chemical environments are similar with six Ga and four Mn atoms as neighbors. All the Mn atoms are equivalent by symmetry and reside in pentagonal prisms, each formed by 10 Ga atoms (two Ga(1) and eight Ga(2)). The bond distances between Mn and the neighboring Ga atoms range from 2.611 to 2.738 Å and ∠(Ga−Mn−Ga) bond angles are from 59.3 to 62.5° along the *c*-axis, as listed in Table 3.

The three-dimensional Ga network is then constructed, first by stacking the $MnGa_{10}$ pentagonal prisms along the *c*-axis so that the prisms share their faces to form pentagonal columns, $MnGa_5$ (Figure 1b). Subsequently, the $MnGa_5$ prisms are aligned in parallel and are fused together by sharing all the five side edges with the neighbors, hence giving the formula, Mn_2Ga_5. In the resulting three-dimensional structure, the Mn atoms form a $3^2{\cdot}4{\cdot}3{\cdot}4$ net in the *ab*-plane, resulting in a triangle−quadrangle−pentagon net $[(3{\cdot}5{\cdot}4{\cdot}5),^2(3{\cdot}5{\cdot}3{\cdot}5)]$ of Ga atoms.[40,41]

(30) Andersen, O. K.; Jepsen, O. *Solid State Commun.* **1971**, *9*, 1763.
(31) Blöchl, P.; Jepsen, O.; Andersen, O. K. *Phys. Rev. B: Condens. Mater. Phys.* **1994**, *34*, 16223.
(32) Lambrecht, W. R. L.; Andersen, O. K. *Phys. Rev. B: Condens. Mater. Phys.* **1986**, *97*, 2439.
(33) Koepernik, K.; Eschrig, H. *Phys. Rev. B: Condens. Mater. Phys.* **1999**, *59*, 1743.
(34) Perdew, J. P.; Wang, Y. *Phys. Rev. B: Condens. Mater. Phys.* **1992**, *45*, 13244.
(35) Hoffmann, R. *J. Chem. Phys.* **1963**, *39*, 1397.
(36) Whangbo, M.-H.; Hoffmann, R.; Woodward, R. B. *Proc. R. Soc. London, Ser. A* **1979**, *366*, 23.
(37) Ren, J.; Liang, W.; Whangbo, M.-H. *CAESAR*; Prime-Color Software, Inc.: Raleigh, NC, 1998.
(38) Rytz, R.; Hoffmann, R. *Inorg. Chem.* **1999**, *38*, 1609.
(39) Canadell, E.; Elsenstein, O. *Organometallics* **1984**, *3*, 759.
(40) O'Keeffe, M.; Hyde, B. G. *Crystal Structures: I. Patterns and Symmetry*; Mineralogical Society of America, Washington: DC, 1996; pp 168−172.
(41) O'Keeffe, M.; Hyde, B. G. *Philos. Trans. R. Soc. London, Ser. A* **1980**, *295*, 553.

Table 4. Relative Energies ΔE (eV/F.U.) of Different Spin States and (Average) Magnetic Moments M (μ_B) on Mn and Ga in Each State of Mn_2Ga_5 Calculated by FPLO Calculations

magnetic state	ΔE	M_{Mn}	M_{Ga}
nonmagnetic	0	0	0
FM	−0.448	2.06	−0.08
AFM1	0.502	±0.55	∼0
AFM2	0.385	±1.87	∼0
AFM3	0.135	±1.81	∼0
AFM4	0.105	±1.94	∼0

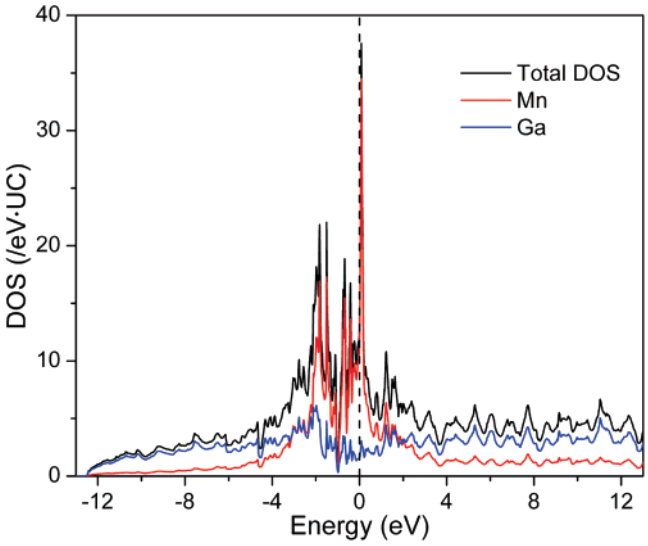

Figure 4. Total and projected DOS (PDOS) plots for the spin-unpolarized state from FPLO calculations. The dashed line indicates the Fermi level, E_F. Black solid line: Total DOS. Red: Mn PDOS. Green: Ga projected DOS. The Mn PDOS dominates on the total DOS near the E_F.

Along the *c*-axis, all Mn (or Ga) atoms form one-dimensional chains with a repeating distance of 2.71 Å. The top and bottom faces of the pentagonal prism are rather large and hence the Mn atoms are in a direct contact through the face openings along the *c*-axis. In the *ab*-plane, however, the Mn atoms are well-separated from each other over 4.5 Å, indicating a strong one-dimensionality, as far as the chemical structure is concerned.

Figure 2a shows the magnetization of the Mn_2Ga_5 in the temperature region from 1.8 to 600 K. The temperature region above 600 K did not show any noticeable change in the magnetization up to 800 K, the maximum temperature in our measurement. The onset of a ferromagnetic transition is found at ∼450 K, which is significantly lower than what was found for the Mn-deficient compound.[23] Below 450 K, the magnetic moment gradually reaches 2.71 μ_B per formula unit as the temperature decreases. In Figure 2b, the hysteresis loop from the magnetization-vs-field measurements at 5 K shows that the compound is a soft magnet with zero remnant field and zero coercivity.

Total Energies and Energy Structure Analysis. The stability of the ferromagnetic state against the nonmagnetic state was confirmed by the FPLO calculations through volume optimization and fixed spin moment calculations. The optimum volume was ca. 10% smaller than the experimental volume at room temperature. The fixed spin moment calculations at the optimized volume showed that a ferromagnetic state with a net magnetic moment of 3.72 μ_B per formula unit has the lowest

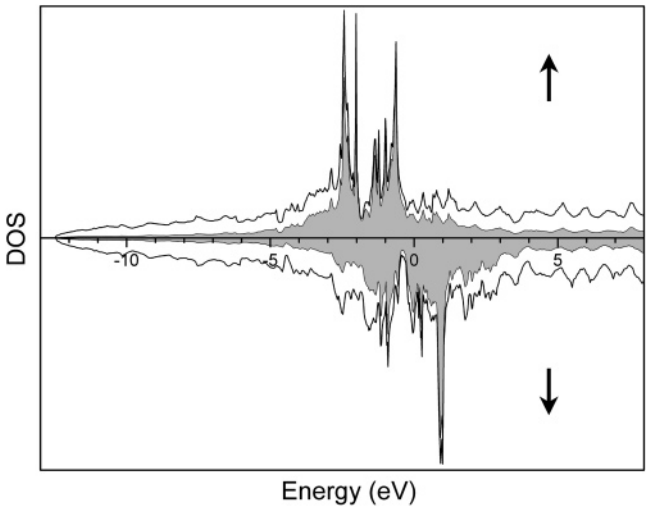

Figure 5. Total DOS and PDOS of Mn (gray area) of the Mn_2Ga_5 in the ferromagnetic state calculated for the volume optimized structure using the FPLO method. The Fermi level is set at 0 eV. Up-spin (majority-spin) channel is shown in the upper panel and down-spin (minority-spin) is in the lower panel.

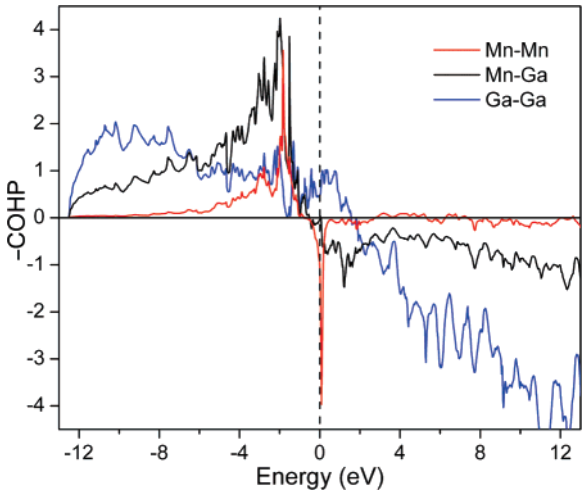

Figure 6. −COHP curves for the Mn−Mn (red solid line), Mn−Ga (black), and Ga−Ga (blue) interactions for the nonmagnetic state of the Mn_2Ga_5. The dashed line indicates E_F.

energy by 0.448 eV per formula unit in comparison to the nonmagnetic state (Table 4). The Ga atoms are also spin-polarized with a small magnetic moment in the direction opposite to the Mn magnetic moment. As shown in Figure 3, four different types of antiferromagnetic (AFM) spin arrangements were considered to compare their stabilities against the ferromagnetic state and the nonmagnetic state of the compound. It was found that all the AFM states have a higher energy than the ferromagnetic state and even the nonmagnetic state (Table 4). Calculation of the magnetic coupling constants was attempted by assuming pairwise interactions, but no consistent values were obtained, indicating that the magnetic exchange interactions are well delocalized.

Figure 4 shows the total DOS and the projected DOSs (PDOSs) of the Mn_2Ga_5 in a nonmagnetic state. The calculated DOS(E_F) of 1.4 states/eV per Mn per spin satisfies the Stoner condition ($I\cdot$ DOS(E_F) = 1.2 with I = 0.84 for Mn), and thus it is in agreement with the existence of the magnetic moment of the Mn atoms. In Figure 4, the total DOS curve shows a

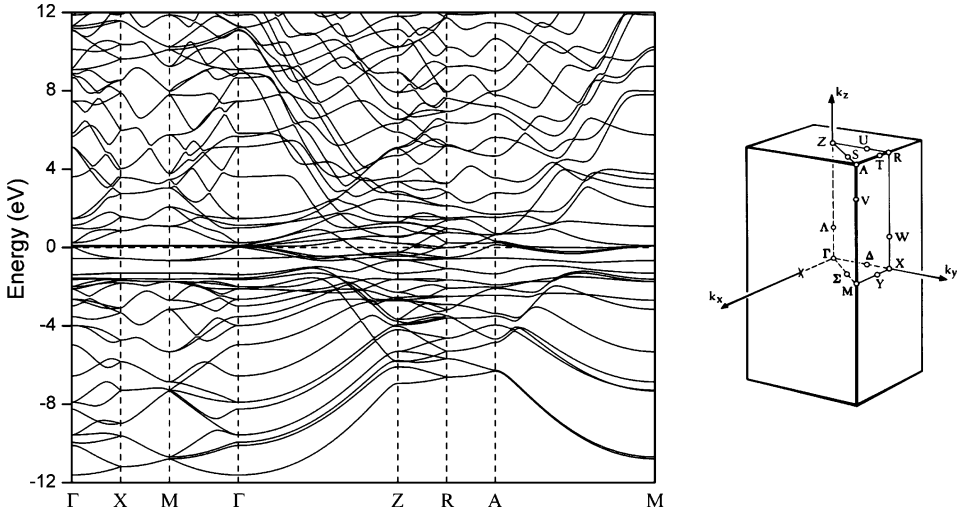

Figure 7. Energy dispersion curves of the nonmagnetic state of the Mn_2Ga_5 calculated for the volume optimized structure with the FPLO method. The first Brillouin zone is shown on the right side with special *k*-points denoted by their symbols.

sharp peak right above the Fermi level, which must cause the unusually high DOS(E_F) for a p-metal-rich intermetallic compound. The PDOS analysis indicates that the sharp peak as well as the surrounding energy region is almost entirely from the Mn atoms and that the Ga atoms contribute more or less evenly throughout the entire energy region. The estimated effective changes on Mn, Ga(1), and Ga(2) are −0.18, +0.13, and +0.06, respectively, from the FPLO calculations and −0.13, +0.17, and +0.03 from the LMTO results. In the ferromagnetic state as shown in Figure 5, the sharp peak splits strongly in the up-spin and down-spin channels. The estimated exchange spitting energy ($\Delta\epsilon$) is 1.7 eV between the sharp Mn peaks, and it is consistent with the fact that the energy bands in that region are essentially from the Mn atoms, as the value holds well the relationship $\Delta\epsilon = I{\cdot}m$.[9−13] The calculated magnetic moment, 3.72 μ_B per formula unit, is rather large in comparison to the observed value of 2.71 μ_B. The overestimation of the magnetic moment is rather unusual in LSDA calculation results in general. It may be due to the unique electronic structure of the compound, which will be described below in detail. The magnetic moments of individual atoms are given in Table 4. A notable feature is a small but negative (i.e., opposite sign) magnetic moment of Ga atoms. Such negative spin polarization cannot be understood strictly from the Stoner theory in which the spin polarization density has uniformly the same direction in real space.

The bonding character of the energy bands were examined for the nonmagnetic state by calculating the crystal orbital hamilton population (−COHPs)[42] for Mn−Mn, Mn−Ga, and Ga−Ga interactions. In Figure 6, the Mn−Ga bonding is well optimized with all bonding bands below the Fermi level and the antibonding bands above it. The Ga−Ga bonding is also almost optimized as only a small portion of the bonding region is not filled in the Ga network. Although not described here, our orbital analysis on the empty Ga network indicates that the optimal number of valence electrons per Ga_5 is 18 ($Ga^{0.6-}$), and yet it may accommodate 14−23 valence electrons ($Ga^{0.2+}$−$Ga^{1.6-}$) because of weak bonding/antibonding nature of the bands near the optimal Fermi level. Meanwhile, the −COHP for Mn−Mn shows a sharp negative peak near the Fermi level that corresponds to the sharp DOS peak in Figure 4, indicating that the orbitals in that energy region are highly antibonding among Mn atoms.

The band dispersion curves are shown in Figure 7 for the nonmagnetic state of the Mn_2Ga_5. While the entangled curves reflect the complexity of the electronic structure of the compound, a notable feature in the figure is that there exist remarkably flat and almost degenerate bands right above the Fermi level. Interestingly, the feature is retained only at the *k*-points on the $k_z = 0$ reciprocal plane, and hence we call it two-dimensional (2D) *superdegeneracy*. Superdegeneracy, a symmetry-driven degeneracy among all the crystal orbitals in the entire Brillouin zone, has been observed in the electronic structures of other compounds with a periodic structure, and it has been attributed to unique atomic orbital phase relationships that result in nonbonding character in the degenerate crystal orbitals.[43] In particular, the superdegeneracy in partially filled π-bands is known to be responsible to the stable ferromagnetic state for some odd-alternant hydrocarbons.[44,45] Not to mention the *partial* superdegeneracy only in a reciprocal plane in this case, the strong antibonding character in the superdegenerate bands of Mn_2Ga_5 is quite unique in contrast to the nonbonding character in other systems. Moreover, such a superdegeneracy, either partial or not, is highly unlikely and has not been reported yet in the band structures of intermetallics, because in those compounds, the orbital interactions are extensive and the atoms are well packed with high coordination numbers.

In order to examine the nature of the superdegenerate bands, we first carried out a fat band analysis for the nonmagnetic state. What is unusual is that among all the Mn valence orbitals, only the $3d_{xz}$ and $3d_{yz}$ orbitals contribute to those bands, as shown in Figure 8 where the band structure is zoomed in near the Fermi level (the Cartesian axes, *x*, *y*, and *z*, are parallel to the *a*-, *b*-, and *c*-axes of the unit cell, respectively). Subsequently, a relevant question is why these Mn $3d_{xz}$ and $3d_{yz}$ orbitals keep exactly the same amount of orbital interactions in all the crystal

(42) Dronskowski, R.; Blöchl, P. *J. Phys. Chem.* **1993**, *97*, 8617.
(43) Hughbanks, T. *J. Am. Chem. Soc.* **1985**, *107*, 6851.
(44) Hughbanks, T.; Kertesz, M. *Mol. Cryst. Liq. Cryst.* **1989**, *176*, 115.
(45) Itoh, K.; Takui, T. *Proc. Jpn. Acad., Ser. B* **2004**, *80*, 29.

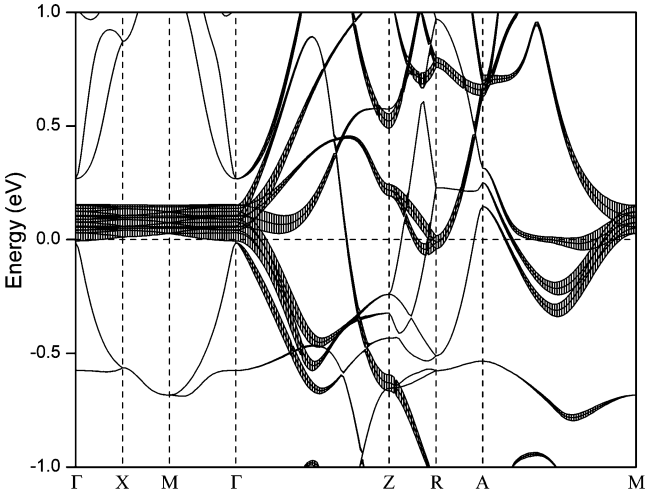

Figure 8. Mn $3d_{xz}$ and $3d_{yz}$ fat bands in the vicinity of the Fermi level of the nonmagnetic state of the Mn_2Ga_5. The bands in the a^*b^* plane are contributed mainly from the Mn ($3d_{xz}$ and $3d_{yz}$) orbitals.

orbitals having $k_z = 0$, so that those crystal orbitals are degenerate. To answer this question, we first consider the phase relationships between the Mn $3d_{xz}$ and $3d_{yz}$ orbitals and the valence orbitals of the surrounding Ga atoms. Only the *k*-points in the reciprocal planes at $k_z = 0$ and $0.5c^*$ are of interest. At those *k*-points, the crystal orbitals must be either symmetric or antisymmetric with respect to the reflection planes perpendicular to the *c*-axis. The symmetry requirement allows us to classify those crystal orbitals into two different types: the ones that are from the Ga *in-plane* orbitals (4s, $4p_x$, and $4p_y$) and the others from the Ga *off-plane* orbital ($4p_z$), in addition to the dominant contribution from the Mn $3d_{xz}$ and $3d_{yz}$. In Figure 9a and b, we depict the phase relationships between the Mn orbitals and the Ga in-plane orbitals for the *k*-vectors in the $k_z = 0$ and $0.5c^*$ planes, respectively. The orientation of the orbitals with respect to the $a(b)$-axis is not important, as it does not change the symmetry property relevant to the reflection planes. In Figure 9a, the Mn and Ga orbitals are orthogonal by symmetry to give net zero orbital interactions and thus no band dispersion (superdegeneracy). In addition, the Mn orbitals interact in an antibonding way along the *c*-axis, in agreement with the COHP curve in Figure 6. Meanwhile, at $k_z = 0.5c^*$ (Figure 9b), those orbitals are no longer orthogonal, and hence the crystal orbitals will have different energies (band dispersion) depending on k_x and k_y. The situation is exactly the opposite for the Ga off-plane orbitals; i.e., they are orthogonal with the Mn orbitals at $k_z = 0.5c^*$, while they are nonorthogonal at $k_z = 0$.

However, a caution is necessary for the expected nonorthogonality in Figure 9c. Figure 10 shows the angular dependence of the overlap integral (*S*) between the Mn $3d_{xz}$ and Ga $4p_z$ orbitals calculated with the extended Hückel method. What is found is that the nodal property of those atomic orbitals causes the *S* value to become zero at $\theta = 28.7$ and 90°. These angles remain the same no matter what orientation the $3d_{xz}$ orbital has with respect to the Ga position (in other words, whichever linear combination of the $3d_{xz}$ and $3d_{yz}$ orbitals interacts with the Ga $4p_z$). Remarkably, θ in the Mn_2Ga_5 structure is found to be 26.7° in average, providing almost zero net interaction between the Mn and Ga orbitals in Figure 9c.

What can be concluded from the previous discussions is that the unique structure of the Mn_2Ga_5 causes the Mn $3d_{xz}$ and $3d_{yz}$ orbitals to have nonbonding interactions with surrounding Ga only for the crystal orbitals at $k_z = 0$ that happen to have their energies close to the Fermi level. As shown by the phase relationships in a and c of Figure 9 as well as the −COHP in Figure 6, these crystal orbitals exhibit a strong antibonding interaction among the Mn atoms along the *c*-axis. However, this antibonding interaction does not cause any significant band dispersion for the crystal orbitals and thus the superdegeneracy can exist. This is because the magnitude of the Mn−Mn antibonding interaction remains the same for all the crystal orbitals at $k_z = 0$ plane since they basically contain only the Mn contribution due to the zero interaction between the Mn and Ga orbitals.

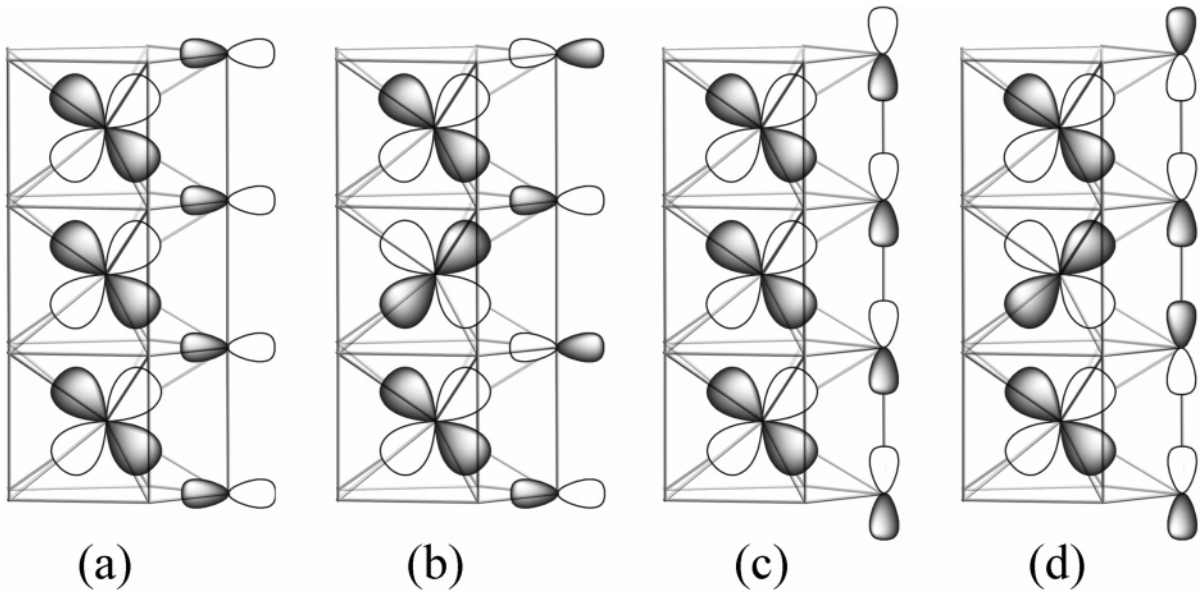

Figure 9. Representative arrangements of Mn $3d_{xz}$ (or d_{yz}) with respect to Ga orbitals. (a) Ga in-plane orbitals at $k_z = 0c^*$ and (b) $k_z = c^*/2$, and (c) Ga off-plane orbitals at $k_z = 0c^*$ and (d) $k_z = c^*/2$.

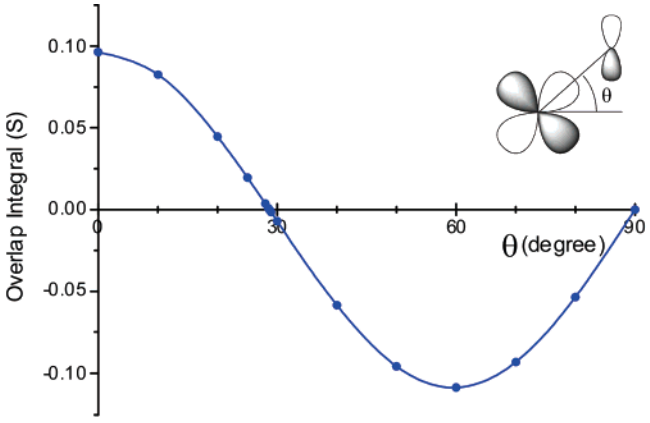

Figure 10. Angular dependence of orbital overlap integral between Mn $3d_{xz}$ and Ga $4p_z$ calculated with the extended Hückel method. The distance between the atoms is fixed at the averaged bond length, d(Mn−Ga) = 2.685 Å. The integral is zero at $\theta = 28.7$ and 90°.

Concluding Remarks

Our work presents the first example of p-metal-rich intermetallic compounds whose ferromagnetism is associated with the remarkable superdegeneracy of transition metal d bands. In contrast to other known p-metal-rich intermetallics, the title compound Mn_2Ga_5 does not utilize all the transition metal d-orbitals in the formation of the structure and the Mn−Ga bonds in particular, leaving some crystal orbitals to exhibit a Mn−Ga nonbonding character in its nonmagnetic electronic structure. The resulting orbital degeneracy near the Fermi level and the high DOS(E_F) value are in agreement with the observed strong ferromagnetism based on the Stoner theory. The existence of the flat (or narrow) bands near the Fermi level resembles the situation of magnetic oxides or magnetic odd-alternant hydrocarbons in that spin polarization takes place in their partially filled nonbonding (or weakly interacting) orbitals. However, the difference is clear: on the contrary to the other magnetic systems, the (super)degeneracy survives only in a localized region of the Brillouin zone in the case of the Mn_2Ga_5, while the band structure in other region fully reflects the complicated nature of the chemical bonding in the Mn_2Ga_5 structure. The Mn−Mn antibonding nature of the superdegenerate bands is quite curious since such bonding character has been conjectured to cause the ferromagnetism.[46,47] While a detailed theoretical work is awaited, the antibonding conjecture can be understood based on the recently developed spin polarization perturbational orbital theory[12] by noting that an antiferromagnetic spin polarization is not favorable when the frontier crystal orbitals have the same phase relationship among magnetic atoms.[48]

Acknowledgment. D.-K.S. is grateful for financial support from the National Science Foundation through his CAREER Award (DMR Contract No. 0239837) and the Camille and Henry Dreyfus Foundation for his Camille Dreyfus Teacher-Scholar Award. We thank Dr. Walter Schnelle in Max Plank Institute for Chemical Physics of Solids, Dresden, Germany, for his magnetic property measurements.

Supporting Information Available: Additional experimental details. This material is available free of charge via the Internet at http://pubs.acs.org.

JA0765924

(46) Goodenough, J. B. *Magnetism and the Chemical Bond*, John Wiley and Sons: New York, 1963; p 298.
(47) Landrum, G. A.; Viklund, P.; Dronskowski, R. *Angew. Chem., Int. Ed.* **2000**, *39*, 1560.
(48) Seo, D.-K. *J. Chem. Phys.* **2007**. In press.